# A Numerical Method for Solving Elliptic Equations on Real Closed Algebraic Curves and Surfaces

Wenrui Hao[1] · Jonathan D. Hauenstein[2] · Margaret H. Regan[3] · Tingting Tang[4]

## Abstract

There are many numerical methods for solving partial different equations (PDEs) on manifolds such as classical implicit, finite difference, finite element, and isogeometric analysis methods which aim at improving the interoperability between finite element method and computer aided design (CAD) software. However, these approaches have difficulty when the domain has singularities since the solution at the singularity may be multivalued. This paper develops a novel numerical approach to solve elliptic PDEs on real, closed, connected, orientable, and almost smooth algebraic curves and surfaces. Our method integrates numerical algebraic geometry, differential geometry, and a finite difference scheme which is demonstrated on several examples.

**Keywords** Partial differential equations · Elliptic equations · Numerical algebraic geometry · Real algebraic geometry

**Mathematics Subject Classification** 65N06 · 65H14 · 68W30

✉ Margaret H. Regan
  mregan@holycross.edu

  Wenrui Hao
  wxh64@psu.edu

  Jonathan D. Hauenstein
  hauenstein@nd.edu

  Tingting Tang
  ttang2@sdsu.edu

1   Department of Mathematics, Penn State University, University Park, PA 16802, USA

2   Department of Applied and Computational Mathematics and Statistics, University of Notre Dame, Notre Dame, IN 46556, USA

3   Department of Mathematics and Computer Science, College of the Holy Cross, Worcester , MA 01610, USA

4   Department of Mathematics and Statistics, San Diego State University, San Diego, CA 92182, USA

## 1 Introduction

Advances in fluid dynamics, biology, material science, and other disciplines have promoted the study of partial differential equations (PDEs) defined on various manifolds. Numerous numerical methods have been developed to solve these PDEs, such as classical implicit [5, 6, 17], finite difference [16, 20, 22], finite element [11, 12, 18], and parameterization methods [21]. In this paper, we specifically consider linear elliptic PDEs defined on closed algebraic curves and surfaces, which are described implicitly as the solution to a system of polynomial equations. We consider the well-posedness of the problem when the domain has singularities corresponding to problems in which variational methods can not be applied. In particular, when the domain is a real closed algebraic curve, we can always reduce the problem to solving an ordinary differential equation (ODE) described in terms of the arc length. Numerically, we can construct a meshing of the curve which is uniform in arc length via numerical algebraic geometry [2, 8]. Such an approach is not limited to smooth curves nor when an a priori global parameterization of the curve is known. From the meshing, we introduce a local tangential parameterization and embed it in a finite difference scheme to numerically solve the problem. A similar approach is extended to real closed algebraic surfaces which are almost smooth, i.e., have at most finitely many singularities.

The linear elliptic PDEs under consideration have the form

$$-\Delta u + c \cdot u = f \qquad \text{on } \Omega \qquad (1)$$

where the operator $\Delta$ is the Laplace–Beltrami operator on a closed domain $\Omega$ while $c$ and $f$ are functions independent of $u$. In particular, we are particularly focused on domains $\Omega$ which are a closed, connected, and orientable $d$-dimensional algebraic set in $\mathbb{R}^n$ where $0 < d < n$. Thus, $\Omega$ is described by the solution set of a system of polynomial equations $F = 0$ on $\mathbb{R}^n$. Curves have $d = 1$ while surfaces have $d = 2$. For example, the unit circle in $\mathbb{R}^2$ as shown in Fig. 1a is a curve defined by the solution set of the polynomial equation $x^2 + y^2 - 1 = 0$ while the unit sphere in $\mathbb{R}^3$ is a surface defined by the solution set of the polynomial equation $x^2 + y^2 + z^2 - 1 = 0$. Moreover, the dimension of the tangent space at each point in $\Omega$ is at least $d$. The smooth points of $\Omega$ are the points where the dimension of the tangent space is equal to $d$ while the singular points are those where the dimension of the tangent space is larger than $d$. For curves ($d = 1$), the number of singular points is always finite, e.g., the lemniscate of Gerono showed in Fig. 1b has one singular point. We only consider surfaces ($d = 2$) where the number of singular points is finite, called *almost smooth* surfaces. The horn torus shown in Fig. 1c is an almost smooth surface with one singular point while the Whitney umbrella shown in Fig. 1d is not an almost smooth surface since it has a line of singularities, i.e., the "handle" of the Whitney umbrella.

For any $d$, if there are no singular points, then $\Omega$ is said to be smooth, i.e., a manifold, and there are many existing numerical methods, e.g., [4–6, 10–12, 16–18, 20–22], for solving (1). For example, [11] considered finite element methods for solving on triangulated surfaces and implicit surface methods using a level set description of the surface. Variational techniques for solving on smooth surfaces based on splines and non-uniform B-splines (NURBS) are reviewed in [4]. Recently, [10] established the theoretical framework to analyze cut finite element methods for the Laplace–Beltrami operator defined on a manifold. These methods focus on smooth surfaces which either can be parameterized or implicitly represented by level sets. In the case of the implicit surface methods, a discretization of the space where the manifold is embedded in is required, which can be inefficient when the codimension, i.e., $n - d$, is high.
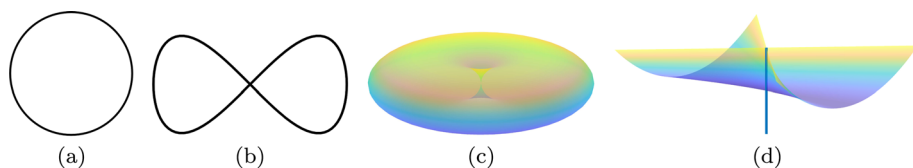
**Fig. 1** **a** Circle, **b** lemniscate of Gerono, **c** horn torus, and **d** Whitney umbrella
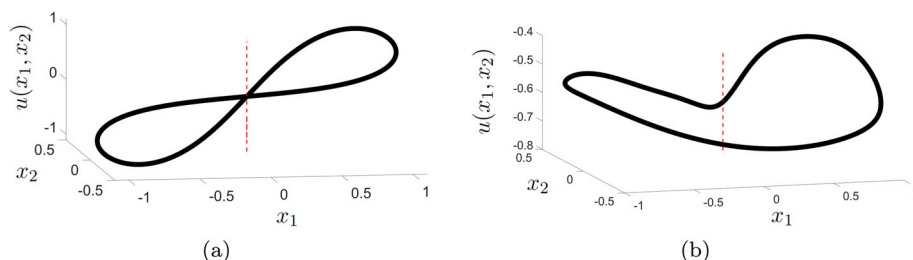


**Fig. 2** Solutions corresponding to (2) on the lemniscate of Gerono where the dashed line corresponds with $(x_1, x_2) = (0, 0)$ showing the first is univalued while the second is multivalued

To the best of our knowledge, little to no studies have been done to investigate the existence of a theoretical or numerical solution on curves with singularities. One possible reason for this is that the solution $u$ to (1) need not take a single value at a singularity of $\Omega$ due to the presence of multiple local irreducible components at a singularity, e.g., the lemniscate of Gerono shown in Fig. 1b has two local irreducible components at the singular point. As an illustration, Fig. 2 shows the solutions to the following two problems

$$(a) - \Delta u + \left( \pi - \frac{4x_1^2 + 4x_2^2 - 3}{8x_1^2 x_2^2 + 16x_2^4 - 3x_1^2 - 17x_2^2 + 4} \right) \cdot u = \pi \cdot x_1 \text{ on } \Omega \tag{2}$$

$$(b) - \Delta u + u = x_1^2 + x_1 x_2 - 1 \text{ on } \Omega \tag{3}$$

where the domain is the lemniscate of Gerono shown in Fig. 1b and defined by

$$\Omega = \{(x_1, x_2) \in \mathbb{R}^2 \mid x_1^4 - x_1^2 + x_2^2 = 0\}.$$

The solution of the former is $u = x_1$ which is univalued at the singularity $(0, 0)$ while the solution of the latter takes two different values at $(0, 0)$, one along each of the two local irreducible components at $(0, 0)$. These problems will be further considered in Exs. 6 and 12, respectively. Numerical algebraic geometry will also be used to compute the local irreducible components [9] to ensure the proper structure of the solution $u$ at the singularities.

The structure of the rest of the paper is as follows. Section 2 shows the existence and uniqueness of the solution to the elliptic problem (1) under certain conditions along with analysis when a global parameterization is known. Sections 3 and 4 describe a local tangential parameterization at smooth points along with considering local irreducible components at singularities.

## 2 Global Parameterization

### 2.1 Formulation

For $k \in \mathbb{N} \cup \{\infty\}$ and a connected set $D \subset \mathbb{R}$, let $C^k(D, \mathbb{R}^n)$ consist of the functions $\alpha : D \to \mathbb{R}^n$ which are $k$-times continuously differentiable on $D$. For $0 \le r \le k$, let $\alpha^{(r)}(t)$ denote the $r^{\text{th}}$ derivative of $\alpha$ at $t$. A real algebraic curve $\Omega \subset \mathbb{R}^n$ is called a *closed parametric $C^k$ curve* if there exists a closed interval $[a, b] \in \mathbb{R}$ and a surjective map $X : [a, b] \to \Omega$ such that $X \in C^k([a, b], \mathbb{R}^n)$ with $X^{(r)}(a) = X^{(r)}(b)$ for all $0 \le r \le k$. If $X$ is also a bijection between $[a, b)$ and $\Omega$, then $\Omega$ is *simple*. A function $h : \Omega \to \mathbb{R}$ is *$k$-times continuously differentiable* on $\Omega$ if $h \circ X \in C^k([a, b], \mathbb{R})$.

**Example 1** The unit circle $\Omega = \{x_1^2 + x_2^2 = 1\} \subset \mathbb{R}^2$ shown in Fig. 1a is a simple closed parametric $C^\infty$ curve. The surjective function $X : [0, 2\pi] \mapsto \Omega$ defined by $X(\theta) = (\cos(\theta), \sin(\theta))$ is infinitely differentiable and bijects $[0, 2\pi)$ onto $\Omega$.

The lemniscate of Gerono $\Lambda = \{x_1^4 - x_1^2 + x_2^2 = 0\} \subset \mathbb{R}^2$ shown in Fig. 1b is a closed parametric $C^\infty$ curve since the surjection $Y : [0, 2\pi] \mapsto \Lambda$ defined by $Y(\theta) = (\cos(\theta), \sin(2\theta)/2)$ is infinitely differentiable. The map $Y$ is not a bijection since $Y(\pi/2) = Y(3\pi/2) = (0, 0)$ which is the self-intersection point. Hence, $\Lambda$ is not a simple curve.

A real algebraic surface $\Omega \subset \mathbb{R}^n$ is called a *closed parametric $C^k$ surface* if, for every $x^* \in \Omega$, there exists a nonempty open connected set $V \subset \mathbb{R}^2$, an open set $U \subset \mathbb{R}^n$ containing $x^*$, and a bijective map $X : V \to U \cap \Omega$ such that $X \in C^k(V, \mathbb{R}^n)$ and the rank of the Jacobian matrix of $X$, denoted $JX$, at every point in $V$ is 2. A function $h : \Omega \to \mathbb{R}$ is *$k$-times continuously differentiable* on $\Omega$ if $h \circ X \in C^k(V, \mathbb{R})$.

**Example 2** The unit sphere $\Omega = \{x_1^2 + x_2^2 + x_3^2 = 1\} \subset \mathbb{R}^3$ is a closed parameteric $C^\infty$ surface. Due to rotational symmetry of the sphere, we only need to consider one point, say $x^* = (0, 0, -1)$. As shown in Fig. 3, one can take $V = \{a_1^2 + a_2^2 < 1/4\} \subset \mathbb{R}^2$, $U = \{x_1^2 + x_2^2 < 1/4\} \subset \mathbb{R}^3$ which clearly contains $x^*$, and bijective map $X : V \to U \cap \Omega$ defined by

$$X(a_1, a_2) = \left( a_1, a_2, -\sqrt{1 - a_1^2 - a_2^2} \right)$$

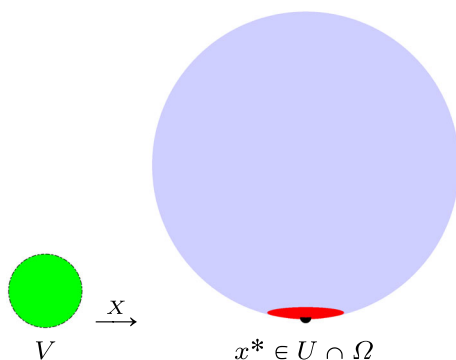which is infinitely differentiable with full rank Jacobian matrix on $V$.

The Whitney umbrella $\Lambda = \{x_1^2 = x_2^2 x_3\} \subset \mathbb{R}^3$ shown in Fig. 1c is not a closed parametric $C^k$ surface for any $k \in \mathbb{N} \cup \{\infty\}$ since, for example, the surface $\Lambda$ near the point $(0, 0, -1)$ is one-dimensional (called the "handle" of the Whitney umbrella).

We now turn to consider (1) on $\Omega \subset \mathbb{R}^n$. Suppose that $G$ is a given metric tensor defined on the smooth points of $\Omega$ with inverse $G^{-1}$. Then, in local coordinates $(t_1, \ldots, t_d)$ where $d = \dim \Omega$,

$$\Delta u = \frac{1}{\sqrt{|g|}} \sum_{i=1}^{d} \frac{\partial}{\partial t_i} \left( \sqrt{|g|} \cdot \sum_{j=1}^{d} g^{ij} \frac{\partial u}{\partial t_j} \right) \tag{4}$$

where $g = \det G$ and $g^{ij}$ is the $(i, j)$ entry of $G^{-1}$.

**Fig. 3** Illustrating a closed parametric map at $x^* = (0, 0, -1)$ on the sphere from Ex. 2



$V \xrightarrow{\quad X \quad} x^* \in U \cap \Omega$

**Example 3** For $\Omega = \mathbb{R}^n$ with the standard metric tensor $G = I_n$, the $n \times n$ identity matrix, the local coordinates are simply the standard coordinates $(x_1, \ldots, x_n)$, $g = \det G = 1$, and $g^{ij} = \delta_{ij}$ (Kronecker delta). Hence,

$$\Delta u = \sum_{i=1}^{n} \frac{\partial^2 u}{\partial x_i^2}$$

which is simply the Laplacian of $u$ on $\mathbb{R}^n$.

**Example 4** Reconsider the unit circle $\Omega = \{x_1^2 + x_2^2 = 1\} \subset \mathbb{R}^2$ with parameterization

$$X(\theta) = (x_1(\theta), x_2(\theta)) = (\cos(\theta), \sin(\theta)) \qquad \text{for } \theta \in [0, 2\pi]$$

from Ex. 1. Since

$$g = \|X'(\theta))\|^2 = \sin^2(\theta) + \cos^2(\theta) = 1,$$

we know that $G = G^{-1} = [1]$. Hence,

$$\Delta u = \frac{d^2 u}{d\theta^2}.$$

For example, if $u(x) = x_1 + x_2$, then $u(\theta) = \cos(\theta) + \sin(\theta)$ with

$$\Delta u = \frac{d^2}{d\theta^2}(\cos(\theta) + \sin(\theta)) = -(\cos(\theta) + \sin(\theta)) = -u.$$

If, instead, we utilize the rational parameterization

$$X(t) = (x_1(t), x_2(t)) = \left(\frac{1-t^2}{1+t^2}, \frac{2t}{1+t^2}\right) \qquad \text{for } t \in \mathbb{R},$$

then

$$g = \|X'(t)\|^2 = \left(\frac{-4t}{(1+t^2)^2}\right)^2 + \left(\frac{2(1-t^2)}{(1+t^2)^2}\right)^2 = \frac{4}{(1+t^2)^2}$$

with $G = [g]$ and $G^{-1} = [g^{-1}]$. Hence,

$$\Delta u = \frac{1+t^2}{2} \frac{d}{dt}\left(\frac{1+t^2}{2}\frac{du}{dt}\right) = \frac{1+t^2}{4}\left((1+t^2)\frac{d^2 u}{dt^2} + 2t\frac{du}{dt}\right) = \frac{(1+t^2)^2}{4}\frac{d^2 u}{dt^2} + \frac{t(1+t^2)}{2}\frac{du}{dt}.$$

Similar as above, if $u(x) = x_1 + x_2$, then $u(t) = (1 + 2t - t^2)/(1 + t^2)$ and one can verify that

$$\Delta u = -\frac{1 + 2t - t^2}{1 + t^2} = -u.$$

***Example 5*** For the unit sphere $\Omega = \{x_1^2 + x_2^2 + x_3^2 = 1\} \subset \mathbb{R}^3$, consider the parameterization

$$X(\theta_1, \theta_2) = (\sin(\theta_1)\cos(\theta_2),\ \sin(\theta_1)\sin(\theta_2),\ \cos(\theta_1)) \qquad \text{for } \theta_1 \in [0, \pi] \text{ and } \theta_2 \in [0, 2\pi].$$

The metric tensor is

$$G = \left[ \frac{\partial x}{\partial \theta_i} \cdot \frac{\partial x}{\partial \theta_j} \right]_{i,j} = \begin{bmatrix} 1 & 0 \\ 0 & \sin^2(\theta_1) \end{bmatrix} \quad \text{with} \quad G^{-1} = \begin{bmatrix} 1 & 0 \\ 0 & \csc^2(\theta_1) \end{bmatrix}$$

yielding $g = \det G = \sin^2(\theta_1)$. Note that since $\theta_1 \in [0, \pi]$, $\sqrt{|g|} = \sin(\theta_1) \geq 0$. Therefore,

$$\Delta u = \frac{1}{\sin(\theta_1)} \left( \frac{\partial}{\partial \theta_1} \left( \sin(\theta_1) \frac{\partial u}{\partial \theta_1} \right) + \frac{\partial}{\partial \theta_2} \left( \sin(\theta_1) \csc^2(\theta_1) \frac{\partial u}{\partial \theta_2} \right) \right)$$

$$= \frac{\partial^2 u}{\partial \theta_1^2} + \csc^2(\theta_1) \frac{\partial^2 u}{\partial \theta_2^2} + \cot(\theta_1) \frac{\partial u}{\partial \theta_1}.$$

For example, if $u(x) = x_1 + x_2 + x_3$, then $u(\theta) = \sin(\theta_1)(\sin(\theta_2) + \cos(\theta_2)) + \cos(\theta_1)$ with

$$\Delta u = -u - \frac{\sin(\theta_2) + \cos(\theta_2)}{\sin(\theta_1)} + \left( \cos^2(\theta_1) \frac{\sin(\theta_2) + \cos(\theta_2)}{\sin \theta_1} - \cos(\theta_1) \right) = -2u.$$

## 2.2 Well-Posedness for Curves

Let $H^1(\Omega)$ denote the Sobolev space with $k = p = 1$ and vanishing boundary set $\Omega$, and $H^{-1}(\Omega)$ denote the dual space to $H^1(\Omega)$. When $\Omega$ is understood, we simply write $H^1$ and $H^{-1}$, respectively.

The following provides our main theoretical result about well-posedness of (1) for curves.

**Theorem 1** *If $\Omega$ is a closed parametric $C^1$ curve and $f, c \in H^{-1}$ with $c \geq 0$ and $\int_\Omega c > 0$, then there exists a unique weak solution $u \in H^1$ to (1).*

***Proof*** We first define a weak solution to (1) by multiplying $v \in H^1$ to both sides of (1) and applying Green's first identity. Hence, for the standard inner product $\langle \cdot, \cdot \rangle$, we have

$$\int_\Omega (-\Delta u + cu)v\,dx = \int_\Omega \langle \nabla u, \nabla v \rangle dx + \int_\Omega cuv\,dx = \int_\Omega fv\,dx. \tag{5}$$

In particular, a function $u \in H^1$ is called a weak solution to (1) if (5) is satisfied for all $v \in H^1$. Consider writing (5) in the following bilinear form:

$$a(u, v) = l(v) \tag{6}$$

where

$$a(u, v) := \int_\Omega \langle \nabla u, \nabla v \rangle dx + \int_\Omega cuv\,dx \quad \text{and} \quad l(v) := \int_\Omega fv\,dx. \tag{7}$$

Then, we can prove (1) has a unique weak solution in $H^1$ using Lax-Milgram Theorem.

Define

$$\langle \alpha, \beta \rangle_{L^2} := \int_\Omega \langle \alpha, \beta \rangle dx \quad \text{and} \quad \langle u, v \rangle_\Omega := \langle \nabla u, \nabla v \rangle_{L^2} + \langle \sqrt{c} \cdot u, \sqrt{c} \cdot v \rangle_{L^2}.$$

The assumptions on $c$ imply that $\langle \cdot, \cdot \rangle_\Omega$ is an inner product. In fact, when $c \equiv 1$, $\langle \cdot, \cdot \rangle_\Omega$ is the default inner product on $H^1$. Let $\| \cdot \|_\Omega$ on $H^1$ be the norm induced by $\langle \cdot, \cdot \rangle_\Omega$. Next, we show the coercivity of the bilinear function $a(\cdot, \cdot)$. To that end, for any $v \in H^1$,

$$a(v, v) = \|\nabla v\|_{L^2}^2 + \|\sqrt{c}v\|_{L^2}^2 = \|v\|_\Omega^2.$$

Given $u, v \in H^1$, we square both sides of (7) and apply the Cauchy-Schwarz inequality to obtain

$$
\begin{aligned}
a(u, v)^2 &= \langle \nabla u, \nabla v \rangle_{L^2}^2 + \left( \int_\Omega cuv dx \right)^2 + 2\langle \nabla u, \nabla v \rangle_{L^2} \int_\Omega cuv dx \\
&\leq \|\nabla u\|_{L^2}^2 \|\nabla v\|_{L^2}^2 + \|\sqrt{c} \cdot u\|_{L^2}^2 \|\sqrt{c} \cdot v\|_{L^2}^2 \\
&\quad + 2\|\nabla u\|_{L^2} \|\nabla v\|_{L^2} \|\sqrt{c} \cdot u\|_{L^2} \|\sqrt{c} \cdot v\|_{L^2} \\
&\leq (\|\nabla u\|_{L^2}^2 + \|\sqrt{c} \cdot u\|_{L^2}^2)(\|\nabla v\|_{L^2}^2 + \|\sqrt{c} \cdot v\|_{L^2}^2) \\
&\leq \|u\|_\Omega^2 \|v\|_\Omega^2
\end{aligned}
$$

which shows the boundedness of $a(\cdot, \cdot)$. Since $f \in H^{-1}$, it follows immediately from the Lax-Milgram Theorem that there exists a unique $u \in H^1$ satisfying (6). □

Theorem 1 extends well-posedness of (1) to some curves which have singularities such as the lemniscate of Gerono shown in Fig. 1b for appropriate choices of $f$ and $c$. In particular, Theorem 1 assumes minimum regularity requirement on $f$ and $c$. In the following examples in Sects. 2.2 and 3, $f$ and $c$ have much nicer properties so that a classical solution exists, which must be the unique solution by Theorem 1. By combining these properties together with Theorem 1 and applying the Sobolev embedding theorem, the solutions to (1) satisfy more regularity conditions leading to the results in Theorem 2 below.

**Example 6** Let $\Lambda$ be the lemniscate of Gerono as in Ex. 1. Consider the linear elliptic PDE

$$-\Delta u + c(x) \cdot u = \pi \cdot x_1 \quad \text{on } \Lambda \quad \text{where } c(x) = \pi - \frac{4x_1^2 + 4x_2^2 - 3}{8x_1^2 x_2^2 + 16x_2^4 - 3x_1^2 - 17x_2^2 + 4}.$$

One can observe that $c \geq 0$ and $\int_\Lambda c > 0$ by considering Fig. 4 which plots $c(X(\theta))$ for $\theta \in [0, 2\pi]$ where $X(\theta) = (\cos(\theta), \sin(2\theta)/2)$ is the global parameterization of $\Lambda$ as in Ex. 1. Hence, Theorem 1 shows that there exists a unique solution to (8). In fact, using (4), it is easy to verify that $u(x) = x_1$ solves (8). This problem will be reconsidered numerically in Ex. 12.

Building on the existence and uniqueness result provided by Theorem 1, the following develops approaches for numerically computing the solution to (1) when a global parameterization is known.

## 2.3 Solving with a Global Parameterization

When the real algebraic curve $\Omega \subset \mathbb{R}^n$ is a closed parametric $C^1$ curve with a given parameterization $X : [a, b] \mapsto \Omega$ such that $X'(t) \neq 0$ for all $t \in [a, b]$, solving (1) reduces to solving an ordinary differential equation on $[a, b]$ with periodic boundary as follows. By
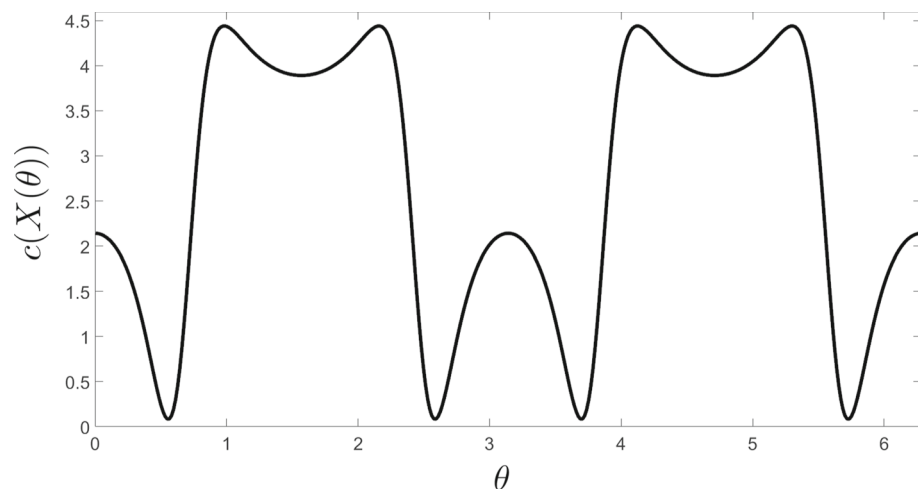
**Fig. 4** Plot of $c(X(\theta))$ with respect to $\theta \in [0, 2\pi]$ from Ex. 6

definition, $g(t) = \|X'(t)\|^2 > 0$, $G(t) = [g(t)]$, and $G^{-1}(t) = [g^{-1}(t)]$ for $t \in [a, b]$. With (4), the linear elliptic PDE (1) simplifies to

$$-\frac{1}{g}\frac{d^2u}{dt^2} + \frac{1}{2g^2}\frac{dg}{dt}\frac{du}{dt} + c \cdot u = f \quad \text{on } [a, b] \tag{8}$$

with periodic boundary where, by abuse of notation, $c$ and $f$ are the corresponding restrictions. Therefore, one can, for example, simply use a finite difference approach with a three-point stencil to discretize (8) as follows. Given $N$, consider $\Delta t = (b - a)/N$ with $t_i = a + i \cdot \Delta t$ for $i = 0, \ldots, N$. Since $u$ is periodic on $[a, b]$ with $t_0 = a$ and $t_N = b$, we aim to compute $u_i$ for $i = 0, \ldots, N - 1$ such that $u_i \approx u(t_i)$ which amounts to computing $U_N = (u_0, \ldots, u_{N-1})^T$ that solves the linear system

$$A_N \cdot U_N = F_N \tag{9}$$

where $F_N = (f(t_0), \ldots, f(t_{N-1}))^T$ and

$$A_N = \begin{pmatrix} C_0 & R_0 & 0 & \cdots & 0 & L_0 \\ L_1 & C_1 & R_1 & 0 & \cdots & 0 \\ 0 & L_2 & C_1 & R_2 & \cdots & 0 \\ \vdots & & \ddots & \ddots & \ddots & \vdots \\ 0 & \cdots & 0 & L_{N-2} & C_{N-2} & R_{N-2} \\ R_{N-1} & 0 & \cdots & 0 & L_{N-1} & C_{N-1} \end{pmatrix} \tag{10}$$

such that

$$L_i = -\frac{1}{g(t_i)\Delta t^2}\left(1 + \frac{g'(t_i)\Delta t}{4g(t_i)}\right), \quad C_i = c(t_i) + \frac{2}{g(t_i)\Delta t^2}, \quad \text{and} \quad R_i = -\frac{1}{g(t_i)\Delta t^2}\left(1 - \frac{g'(t_i)\Delta t}{4g(t_i)}\right).$$

By imposing a stronger condition on the regularity of the solution $u$ to (1), namely $u \in C^4(\Omega) \subset H^1$, we obtain the following.

**Theorem 2** *If $u \in C^4(\Omega)$ and there exists $\delta > 0$ such that $c > \delta$, then the numerical scheme (9) is convergent, stable, and has second order accuracy.*

***Proof*** Using Taylor series expansion, we have

$$u(x(t_{i+1})) = u(x(t_i)) + \Delta t u'(x(t_i)) + \frac{\Delta t^2}{2} u''(x(t_i)) + \frac{\Delta t^3}{3!} u'''(x(t_i)) + \frac{\Delta t^4}{4!} u''''(x(\eta_i)),$$
$$u(x(t_{i-1})) = u(x(t_i)) - \Delta t u'(x(t_i)) + \frac{\Delta t^2}{2} u''(x(t_i)) - \frac{\Delta t^3}{3!} u'''(x(t_i)) + \frac{\Delta t^4}{4!} u''''(x(\xi_i)),$$

$$(11)$$

where $\eta_i \in [t_i, t_{i+1}]$ and $\xi_i \in [t_{i-1}, t_i]$. Therefore,

$$\frac{u(x(t_{i+1})) - 2u(x(t_i)) + u(x(t_{i-1}))}{\Delta t^2} = u''(x(t_i)) - \frac{\Delta t^2}{4!}(u''''(x(\eta_i)) + u''''(x(\xi_i))).$$

This expression combined with (9) yields

$$A_N \begin{pmatrix} u(x(t_0)) \\ \vdots \\ u(x(t_{N-1})) \end{pmatrix} + \frac{\Delta t^2}{4!} \begin{pmatrix} u''''(x(\eta_0)) + u''''(x(\xi_0)) \\ \vdots \\ u''''(x(\eta_{N-1})) + u''''(x(\xi_{N-1})) \end{pmatrix} = F_N. \qquad (12)$$

Denoting

$$u_N = \begin{pmatrix} u(x(t_0)) \\ \vdots \\ u(x(t_{N-1})) \end{pmatrix} \quad \text{and} \quad u_N'''' = \begin{pmatrix} u''''(x(\eta_0)) + u''''(x(\xi_0)) \\ \vdots \\ u''''(x(\eta_{N-1})) + u''''(x(\xi_{N-1})) \end{pmatrix},$$

subtracting (9) from (12) yields

$$A_N(u_N - U_N) = -\frac{\Delta t^2}{4!} u_N''''.$$

Thus, the error satisfies

$$\|u_N - U_N\|_\infty = \frac{\Delta t^2}{4!} \|A_N^{-1} u_N''''\|_\infty \le \frac{\Delta t^2}{4!} \|A_N^{-1}\|_\infty \|u_N''''\|_\infty. \qquad (13)$$

For sufficiently small $\Delta t$, one can assume that $C_i > \delta + \frac{2}{g(t_i)\Delta t^2} > 0$ while both $|L_i|$ and $|R_i|$ are bounded above by, say, $\frac{\delta}{4} + \frac{1}{g(t_i)\Delta t^2}$. Thus, we have

$$C_i - (|L_i| + |R_i|) > \frac{\delta}{2} > 0.$$

Hence, $A_N$ is a strictly diagonally dominant matrix so that $A_N$ is invertible where the real parts of the eigenvalues are positive so the stability of the scheme follows immediately. Moreover, the Ahlberg-Nilson-Varah bound [13, 14] yields $\|A_N^{-1}\|_\infty \le \frac{2}{\delta} < \infty$ showing that

$$\|u_N - U_N\|_\infty \le \frac{2 \cdot \Delta t^2}{\delta \cdot 4!} \|u_N''''\|_\infty.$$

Since $u \in C^4(\Omega)$, the global error defined above for scheme (9) is bounded and converges to 0 as the mesh size goes to zero. In particular, the scheme is convergent with second order accuracy. $\qquad \square$

Of course, one can repeat this construction using a larger stencil and imposing a stronger condition on the regularity of the solution to obtain higher order accuracy. The following illustrates the convergence rate for the three-point stencil using a five-point stencil with many points to estimate the error.

**Table 1** Comparison of error for solving (14) using the global parameterization (15)

| $N$ | $L_\infty$ error | Order |
|---|---|---|
| 160 | $2.043 \times 10^{-4}$ | – |
| 320 | $5.099 \times 10^{-5}$ | 2.002 |
| 640 | $1.274 \times 10^{-5}$ | 2.000 |
| 1280 | $3.185 \times 10^{-6}$ | 2.000 |

***Example 7*** Consider solving

$$- \Delta u + u = x \quad \text{on} \quad x^2 + 50y^2 = 1. \tag{14}$$

Using the global parameterization

$$X(\theta) = \left( \sin\theta, \frac{\cos\theta}{\sqrt{50}} \right), \qquad \theta \in [0, 2\pi], \tag{15}$$

one aims to solve

$$-\frac{50}{50 - 49\sin^2\theta} u_{\theta\theta} - \frac{2450\sin\theta\cos\theta}{(50 - 49\sin^2\theta)^2} u_\theta + u = \sin\theta \quad \text{on } [0, 2\pi]$$

such that $u$ is periodic on $[0, 2\pi]$. Table 1 lists the error and convergence order which computationally verifies second order convergence as expected by Theorem 2. Here, the error is computed by comparing against the solution obtained using a five-point stencil with $N = 20,480$.

# 3 Local Parameterization for Curves

When there is no readily available global parameterization, one can solve (1) via a finite difference method based on local parameterization at each sample point. The following proceeds by first considering a numerical cell decomposition using numerical algebraic geometry, then analyzing a local tangential parameterization at smooth points, and finally considering singular points.
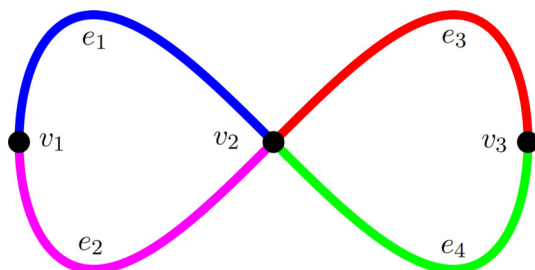
## 3.1 Curve Decomposition Using Numerical Algebraic Geometry

One approach for decomposing a curve is to utilize a numerical cellular decomposition [8, 15] computed using numerical algebraic geometry [3, 19]. A cellular decomposition of a curve is a disjoint union of finitely many vertices $V$, which are simply points on the curve, and edges $E$, which are portions of the curve diffeomorphic to an interval in $\mathbb{R}$. The endpoints of each edge are vertices. In particular, $V$ must contain the set of singular points of the curve.

***Example 8*** Reconsider the lemniscate of Gerono $\Lambda \subset \mathbb{R}^2$ defined in Ex. 1 and shown in Fig. 2b. Figure 5 illustrates a cellular decomposition of $\Lambda$ consisting of 3 vertices and 4 edges.

A numerical cellular decomposition simply represents each edge of a cellular decomposition by an interior point along with a homotopy that permits the tracking along the edge starting from the interior point. From this numerical representation, one can perform computations on each edge. For example, one can sample points along each edge and construct

**Fig. 5** Cellular decomposition for lemniscate of Gerono with vertices $v_i$ and edges $e_j$



a Chebyshev interpolant as described in [1]. From the Chebyshev interpolant, one can easily approximate the arc length of each edge and approximate mesh points in the desired structure, for example, uniform in arc length.

At each point on the curve, there is a local irreducible decomposition of the curve at the point which can be computed using numerical algebraic geometry [9]. A curve is locally irreducible at every smooth point on the curve and is locally diffeomorphic to the tangent line. This is utilized next to construct a tangential parameterization at smooth points. The only points on a curve where the curve could be locally reducible is at a singular point. Hence, at each singular point on the curve, the approach in [9] uses the local monodromy group structure computed using a homotopy to determine the locally irreducible components of the curve at a singular point. Moreover, each locally irreducible component has a well-defined local degree [9]. If a component has local degree equal to 1, then it is locally diffeomorphic to a tangent line.

**Example 9** Continuing from Ex. 8, all points are smooth points of $\Lambda$ except $v_2 = (0, 0)$. At $v_2$, $\Lambda$ decomposes into two locally irreducible components each of local degree 1 corresponding to each of the two local tangent directions at $v_2$.

Local irreducible decomposition is important for solving (1) since Theorem 1 enforces that the solution is continuous along each locally irreducible component. Hence, a numerical solving scheme needs to allow for a singular point to take a different value along each locally irreducible component passing through the singular point as illustrated in Fig. 2b.

## 3.2 Tangential Parameterization at Smooth Points

The following uses an approach based on a local tangential parameterization for a smooth curve to compute $x'(s)$ and obtain $g$ which greatly simplifies the calculation of coefficients for the numerical scheme. Let $\pi_N = \{p_0, p_1, \ldots, p_{N-1}\}$ consist of $N$ mesh points uniformly distributed in arc length using a cyclic ordering with $p_i = p_{N+i}$ as needed. Define $[p_{i-1}, p_{i+1}]$ to be the segment of the curve passing through points $p_{i-1}, p_i$, and $p_{i+1}$. Let $v_i$ be a unit tangent vector to the curve at $p_i$ and consider $\ell_i(t) = p_i + tv_i$ which parameterizes the tangent line to the curve at $p_i$. Consider the map $\alpha_i : [p_{i-1}, p_{i+1}] \to \mathbb{R}$ defined by $\alpha_i(p) = (p - p_i) \cdot v_i$. By replacing $v_i$ by $-v_i$ as needed and taking $N$ large enough, $\alpha_i$ is a diffeomorphism from $[p_{i-1}, p_{i+1}]$ to $[\alpha_i(p_{i-1}), \alpha_i(p_{i+1})]$ where

$$\alpha_i(p_{i-1}) < 0 = \alpha_i(p_i) < \alpha_i(p_{i+1}).$$

Note that smoothness and a fine enough discretization, i.e., taking $N$ large enough, are essential for constructing such local diffeomorphisms. Figure 6 provides an illustration of this local tangential parameterization construction.
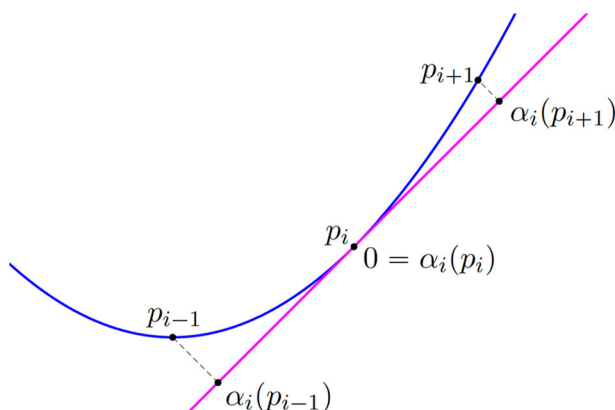
**Fig. 6** Illustration of tangential parameterization

Let $X_i : [\alpha_i(p_{i-1}), \alpha_i(p_{i+1})] \to [p_{i-1}, p_{i+1}]$ be the inverse of $\alpha_i$. Locally, (8) using $X_i(t)$ is simplified at $t = 0$ based on the following.

**Theorem 3** *With the setup described above, $X_i'(0) = v_i$. Moreover, for corresponding metric tensor $G(t)$, (4) becomes $\Delta u(0) = \frac{\partial^2 u(0)}{\partial t^2}$.*

**Proof** For $t \in [\alpha_i(p_{i-1}), \alpha_i(p_{i+1})]$, one knows that $X_i(t)$ satisfies

$$\begin{bmatrix} (X_i(t) - p_i) \cdot v_i - t \\ F(X_i(t)) \end{bmatrix} = 0.$$

By the implicit function theorem,

$$X_i'(t) = -\begin{bmatrix} v_i^T \\ JF(X_i(t)) \end{bmatrix}^{-1} \begin{bmatrix} -1 \\ 0 \end{bmatrix}. \tag{16}$$

Since $v_i \cdot v_i = 1$ and $JF(X_i(0))v_i = 0$, it immediately follows from (16) that $X_i'(0) = v_i$. With $g(t) = G(t) = \|X_i'(t)\|^2$, $g_i(0) = 1$. Additionally, from the first row of (16), we know $v_i \cdot X_i'(t) = 1$ so that $v_i \cdot X_i''(t) = 0$. Hence, at $t = 0$, $X_i'(0) \cdot X_i''(0) = v_i \cdot X_i''(0) = 0$ which immediately yields that $\frac{dg_i(0)}{dt} = 0$ and the result follows. $\square$

**Example 10** To illustrate, consider the ellipse $x^2 + 10y^2 = 1$ at

$$p = \begin{bmatrix} 1 \\ 0 \end{bmatrix} \text{ with } v = \begin{bmatrix} 0 \\ 1 \end{bmatrix} \text{ so that } X(t) = \begin{bmatrix} \sqrt{1 - 10t^2} \\ t \end{bmatrix}.$$

it is clear that $X'(0) = v$. Moreover, for $t$ near 0, (4) becomes

$$\Delta u(t) = \sqrt{\frac{1 - 10t^2}{1 + 90t^2}} \cdot \frac{d}{dt}\left(\sqrt{\frac{1 - 10t^2}{1 + 90t^2}}\frac{du(t)}{dt}\right) = \frac{1 - 10t^2}{1 + 90t^2}\frac{d^2u(t)}{dt^2} - \frac{100t}{(1 + 90t^2)^2}\frac{du(t)}{dt}$$

which yields $\Delta u(0) = \frac{d^2u(0)}{dt^2}$ in accordance with Theorem 3.

Combining with (8), one can develop a local discretization to approximate $u(p_i)$ for each $i$ which is simplified due to Theorem 3. For example, with $u_i \approx u(p_i)$, a three-point stencil

**Table 2** Comparison of global and local parameterization methods for solving (18) when $a = 50$

| N | Global parameterization | | Local tangential parameterization | |
|---|---|---|---|---|
| | $L_\infty$ error | Order | $L_\infty$ error | Order |
| 160 | $2.043 \times 10^{-4}$ | – | $2.459 \times 10^{-3}$ | – |
| 320 | $5.099 \times 10^{-5}$ | 2.002 | $6.401 \times 10^{-4}$ | 1.942 |
| 640 | $1.274 \times 10^{-5}$ | 2.000 | $1.630 \times 10^{-4}$ | 1.975 |
| 1280 | $3.185 \times 10^{-6}$ | 2.000 | $4.094 \times 10^{-5}$ | 1.992 |

yields the following discretization:

$$L_i \cdot u_{i-1} + C_i \cdot u_i + R_i \cdot u_{i+1} = f(p_i) \tag{17}$$

where

$$L_i = \frac{-2}{\alpha_i(p_{i-1})(\alpha_i(p_{i-1}) - \alpha_i(p_{i+1}))}, \quad C_i = c(p_i) + \frac{-2}{\alpha_i(p_{i+1})\alpha_i(p_{i-1})},$$

$$R_i = \frac{-2}{\alpha_i(p_{i+1})(\alpha_i(p_{i+1}) - \alpha_i(p_{i-1}))}.$$

Writing $U_N = (u_0, \ldots, u_{N-1})^T$, and $F_N = (f(p_0), \ldots, f(p_{N-1}))^T$, (17) yields the linear system

$$B_N \cdot U_N = F_N$$

where $B_N$ is the same as $A_N$ in (10) with the localized versions of $L_i$, $C_i$, and $R_i$ above. In particular, note that this does not require computing $g_i$.

**Theorem 4** *If $u \in C^3(\Omega)$ and there exists $\delta > 0$ such that $c > \delta$, the finite difference scheme arising from (17) is convergent and at least first order accurate in arc length mesh size.*

**Proof** The proof is similar to that of Theorem 2 except that (17) uses an unstructured three-point stencil to approximate $\Delta u(p_i)$, which becomes the second-order central difference scheme when $\alpha_i(p_{i+1}) = -\alpha_i(p_i)$. □

**Remark 1** By imposing a stronger condition on the regularity of the solution $u$ as well as increasing the size of the domain $\alpha_i$ for which each remains a diffeomorphism, one can naturally replace the three-point stencil used in (17) with larger stencils and obtain similar results to Theorem 4 with higher-order convergence.

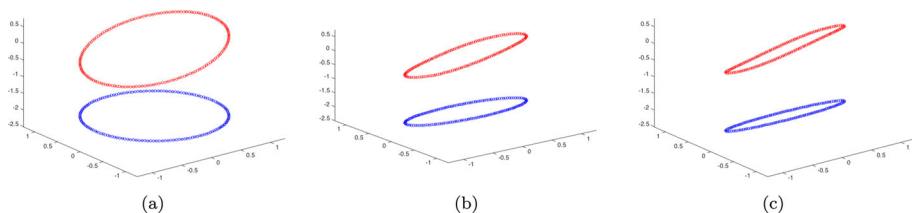**Example 11** For $a > 0$, consider solving

$$-\Delta u + u = x \quad \text{on } x^2 + ay^2 = 1. \tag{18}$$

Using the global parameterization $\left( \cos t, \frac{\sin t}{\sqrt{a}} \right)$ of the ellipse, we first compare the global method in Sect. 2.3 with the local tangential parameterization. Table 2 compares using a three-point stencil for both when $a = 50$ where the errors are computed by comparing against an approximate solution computed using a five-point stencil with the global parameterization using 20,480 points.

We next compare using a three-point stencil and a five-point stencil with the local tangential parameterization for $a = 1$, $a = 10$, and $a = 50$. The results are summarized in Table 3

**Table 3** Comparison of using the local tangential parameterization method for different stencil sizes and varying values of $a$ when solving (18)

| | $N$ | 3-point stencil | | 5-point stencil | |
|---|---|---|---|---|---|
| | | $L_\infty$ error | Order | $L_\infty$ error | Order |
| $a = 1$ | 160 | $9.639 \times 10^{-5}$ | – | $2.979 \times 10^{-7}$ | – |
| | 320 | $2.410 \times 10^{-5}$ | 2.000 | $1.859 \times 10^{-8}$ | 4.002 |
| | 640 | $6.024 \times 10^{-6}$ | 2.000 | $1.162 \times 10^{-9}$ | 4.000 |
| | 1280 | $1.506 \times 10^{-6}$ | 2.000 | $7.322 \times 10^{-11}$ | 3.988 |
| $a = 10$ | 160 | $5.744 \times 10^{-4}$ | – | $5.191 \times 10^{-5}$ | – |
| | 320 | $1.442 \times 10^{-4}$ | 1.995 | $3.265 \times 10^{-6}$ | 3.991 |
| | 640 | $3.607 \times 10^{-5}$ | 1.999 | $2.046 \times 10^{-7}$ | 3.997 |
| | 1280 | $9.020 \times 10^{-6}$ | 2.000 | $1.281 \times 10^{-8}$ | 3.998 |
| $a = 50$ | 160 | $2.459 \times 10^{-3}$ | – | $7.394 \times 10^{-3}$ | – |
| | 320 | $6.401 \times 10^{-4}$ | 1.942 | $3.119 \times 10^{-4}$ | 4.567 |
| | 640 | $1.630 \times 10^{-4}$ | 1.975 | $1.968 \times 10^{-5}$ | 3.986 |
| | 1280 | $4.094 \times 10^{-5}$ | 1.992 | $1.245 \times 10^{-6}$ | 3.983 |



**Fig. 7** Solution (red) for $-\Delta u + u = x$ on $x^2 + ay^2 = 1$ (blue) with $N = 160$ mesh points for **a** $a = 1$, **b** $a = 10$, and **c** $a = 50$ (Color figure online)

with the error computed as above. This shows that the error decreases when curvature is more uniform throughout the curve so that the unstructured stencil approaches a uniformly-spaced stencil. Figure 7 shows the numerical solutions of (18) for these three instances using $N = 160$ points.
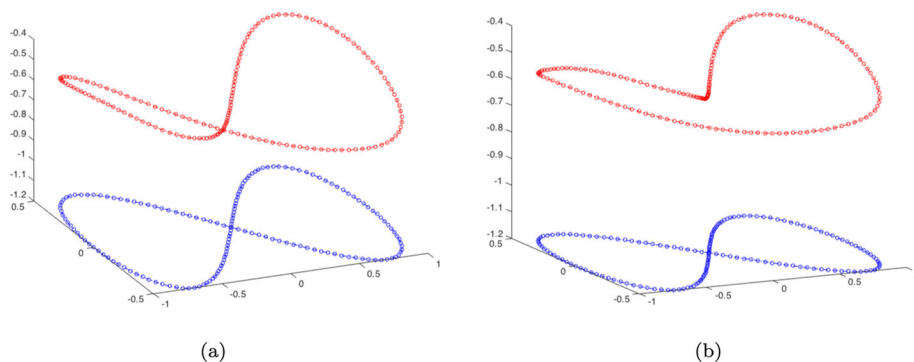
**Remark 2** Using Theorem 3, this local tangential approximation does not encounter the cost of approximating metric tensor coefficients. Moreover, by using numerical algebraic geometry to perform computations on the curve $\Omega \subset \mathbb{R}^n$, we note that we are solving in the space of $H^1(\Omega)$ instead of the higher-dimensional space $H^1(\mathbb{R}^n)$. This becomes especially useful for large $n$.

### 3.3 Local Parameterization Near Singularities

For a smooth curve, every point has a well-defined tangent direction and the curve has a local tangential parameterization as illustrated in Fig. 6. For a singular point, one needs to look at each local irreducible component and allow the value of $u$ at the singular point to take a different value along each such component as described in Sect. 3.1. If a local irreducible component has local degree 1, it is locally diffeomorphic to a well-defined tangent line so

**Table 4** Error analysis when using the local parameterization with a three-point stencil when solving (8)

| $N$ | $L_\infty$ error | Order |
|---|---|---|
| 160 | $3.815 \times 10^{-4}$ | – |
| 320 | $9.391 \times 10^{-5}$ | 2.022 |
| 640 | $2.330 \times 10^{-5}$ | 2.011 |
| 1280 | $6.116 \times 10^{-6}$ | 1.930 |



(a)                              (b)

**Fig. 8** Solution (red) for $-\Delta u + u = x^2 + xy - 1$ on $x^4 - x^2 + y^2 = 0$ (blue) with $N = 160$ points using a three-point stencil, where (**a**) and (**b**) are different views of the same solution (Color figure online)

that the singular point is a smooth point with respect to the local irreducible component. Hence, one can simply apply the local tangential parameterization from Sect. 3.2 along the local irreducible component.

**Example 12** Consider the following problem

$$- \Delta u + u = f(x, y) \quad \text{on } x^4 - x^2 + y^2 = 0 \tag{19}$$

where $f(x, y) = x^2 + xy - 1$ whose solution was shown in Fig. 2b. The origin is the only singular point on the lemniscate of Gerono which arises as the intersection of two locally irreducible components of local degree 1 so that one can employ a local tangential parameterization along each locally irreducible component. Table 4 summarizes the results when using a local tangential parameterization with a three-point stencil where the errors are computed using a three-point stencil with the global parameterization from Ex. 1 with $N = 20,480$ points. Figure 8 shows two views of the solution computed using $N = 160$ points.

When the local degree of a local irreducible component is more than 1, one can, for example, use a truncated Puiseux series expansion where the coefficients can be computed using numerical algebraic geometry. Moreover, by reparameterizing (e.g., see [19, § 10.2.2]), the Puiseux series expansion is transformed into a power series expansion and thus one can use a truncated power series expansion. Such a truncated expansion yields an approximation of a local parameterization of the local irreducible component near the singularity. Then, one can use a discretization of (8) with this approximate local parameterization near the singularity and use a local tangential parameterization away from the singularity.

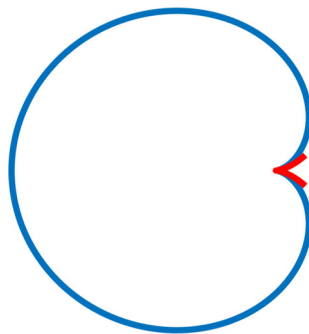**Fig. 9** Cardioid (blue) along with approximation (red) near the singularity at the origin (Color figure online)



**Table 5** Error analysis for solving (20)

| $N$ | $L_\infty$ error | Order |
|-----|------------------|-------|
| 60  | $2.826 \times 10^{-5}$ | – |
| 80  | $2.348 \times 10^{-6}$ | 8.648 |
| 100 | $3.656 \times 10^{-7}$ | 8.334 |
| 120 | $8.196 \times 10^{-8}$ | 8.202 |
| 140 | $2.339 \times 10^{-8}$ | 8.134 |

**Example 13** Consider the following problem

$$-\Delta u + u = f(x, y) \quad \text{on } (x^2 + y^2)^2 + 4x(x^2 + y^2) - 4y^2 = 0, \quad (20)$$

where $f(x, y) = (3607x^2 - 224xy^2 + 7662x - 53y^2 - 973)/(196x^2 + 616x + 196y^2 + 1112)$. The curve is called a cardioid (shown in blue in Figs. 9 and 10) which has a locally irreducible cusp at the origin of local degree 2. The choice of $f$ was selected so that (20) has an exact solution of $u(x, y) = x + x^2$ which is used for error analysis provided in Table 5. In particular, to demonstrate higher-order methods, we used an eighth-order method with a local tangential approximation away from the singularity. Near the singularity, we approximated $x(y)$ so that $F(x(y), y) = 0$. Since $x(y)$ is a Puiseux series where the denominator is 3, reparameterizing $y = s^3$ yields that $x(s)$ is power series in $s$ with the first few terms being

$$x(s) = s^2 - \frac{5}{12}s^4 - \frac{1}{16}s^6 - \frac{91}{5184}s^8 + \cdots.$$

To ensure more than enough accuracy, we used a degree 58 expansion which is pictorially shown in Fig. 9 coupled with a tenth-order discretization at the singularity. Figure 10 shows the numerical solution of (20) computed using $N = 60$ points. Since this computation was performed using double precision, the value of $N$ needs to be large enough to show convergence of the method but small enough to avoid numerical ill-conditioning.

## 4 Local Parameterization for Surfaces

For smooth surfaces with a known global parameterization, there exist well-studied methods to solve (1) as highlighted in the Introduction. As in Sect. 3 when considering curves, we focus on the case when there is no readily available global parameterization.
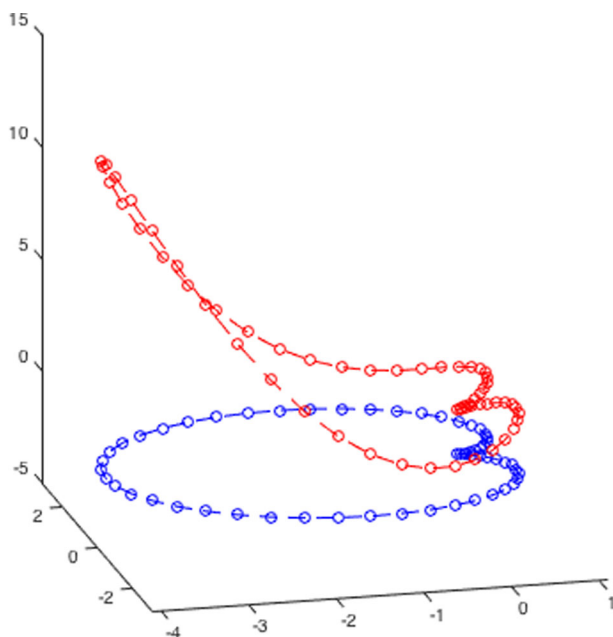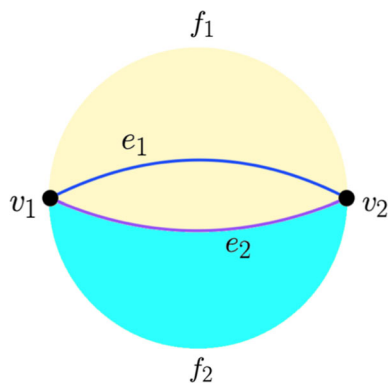
**Fig. 10** Solution (red) for (20) of a cardioid (blue) using $N = 60$ points (Color figure online)

**Fig. 11** Surface decomposition for a sphere with vertices $v_i$, edges $e_j$, and faces $f_k$



## 4.1 Surface Decomposition Using Numerical Algebraic Geometry

The extension of Sect. 3.1 to a surface is a cellular decomposition consisting of finitely many faces $F$, which are portions of the surface diffeomorphic to a rectangle in $\mathbb{R}^2$, along with edges $E$ and vertices $V$. In particular, the boundary of each face consists of finitely many edges, each of which has a vertex at each end.

**Example 14** A cellular decomposition of a sphere consisting of 2 vertices, 2 edges, and 2 faces is illustrated in Fig. 11.

A numerical cellular decomposition, as first described in [7], represents each face by an interior point along with a homotopy that permits the tracking along the face starting from the interior point. The same holds for edges as summarized in Sect. 3.1.

### 4.2 Tangential Parameterization at Smooth Points

By simply adapting the approach in Sect. 3.2 from a local parameterization based on the tangent line for a curve to a local parameterization based on the tangent plane for a surface, the following obtains an analog of Theorem 3 for the surface case.

Suppose that $p$ is a smooth point on the surface $\Omega \subset \mathbb{R}^n$ such that $w_1, w_2 \in \mathbb{R}^n$ span the tangent space with $w_i \cdot w_j = \delta_{ij}$. Hence, the tangent space is parameterized by $\ell(t) = p + t_1 w_1 + t_2 w_2$. Let $\alpha : \Omega \to \mathbb{R}^2$ where $\alpha(q) = ((q - p) \cdot w_1, (q - p) \cdot w_2)$. On $\Omega$ locally nearly $p$, $\alpha$ has an inverse, say, $X(t) = X(t_1, t_2)$ where $X(0) = p$. As with curves, smoothness with a local viewpoint, e.g., mesh points with a sufficiently fine discretization, are essential for constructing such local diffeomorphisms.

**Theorem 5** *With the setup described above, $\frac{\partial X(0)}{\partial t_i} = w_i$. Moreover, for corresponding metric tensor $G(t)$, (4) becomes*

$$\Delta u(0) = \frac{\partial^2 u(0)}{\partial t_1^2} + \frac{\partial^2 u(0)}{\partial t_2^2}.$$

**Proof** The corresponding system that $X(t)$ satisfies is

$$\begin{bmatrix} (X(t) - p) \cdot w_1 - t_1 \\ (X(t) - p) \cdot w_2 - t_2 \\ F(X(t)) \end{bmatrix} = 0.$$

By the implicit function theorem,

$$\begin{bmatrix} \frac{\partial X(t)}{\partial t_1} & \frac{\partial X(t)}{\partial t_2} \end{bmatrix} = - \begin{bmatrix} w_1^T \\ w_2^T \\ JF(X(t)) \end{bmatrix}^{-1} \begin{bmatrix} -1 & 0 \\ 0 & -1 \\ 0 & 0 \end{bmatrix}.$$

Since $JF(X(0))w_i = 0$ and $w_i \cdot w_j = \delta_{ij}$, one has $\frac{\partial X(0)}{\partial t_i} = w_i$ and $w_i \cdot \frac{\partial X(t)}{\partial t_j} = \delta_{ij}$. Hence,

$$w_i \cdot \frac{\partial^2 X(t)}{\partial t_j \partial t_k} = 0. \tag{21}$$

By definition, the metric tensor and its inverse are

$$G(t) = \begin{bmatrix} \frac{\partial X(t)}{\partial t_1} \cdot \frac{\partial X(t)}{\partial t_1} & \frac{\partial X(t)}{\partial t_1} \cdot \frac{\partial X(t)}{\partial t_2} \\ \frac{\partial X(t)}{\partial t_2} \cdot \frac{\partial X(t)}{\partial t_1} & \frac{\partial X(t)}{\partial t_2} \cdot \frac{\partial X(t)}{\partial t_2} \end{bmatrix} \text{ and } G^{-1}(t) = \frac{1}{g(t)} \begin{bmatrix} \frac{\partial X(t)}{\partial t_2} \cdot \frac{\partial X(t)}{\partial t_2} & -\frac{\partial X(t)}{\partial t_2} \cdot \frac{\partial X(t)}{\partial t_1} \\ -\frac{\partial X(t)}{\partial t_1} \cdot \frac{\partial X(t)}{\partial t_2} & \frac{\partial X(t)}{\partial t_1} \cdot \frac{\partial X(t)}{\partial t_1} \end{bmatrix}$$

where $g(t) = \det G(t)$. Hence, $G(0) = G^{-1}(0) = I_2$ and $g(0) = 1$. Moreover, it follows from (21) that $\frac{\partial g(0)}{\partial t_i} = 0$ and $\frac{\partial g^{ij}(0)}{\partial t_i} = 0$ where $g^{ij}(t)$ is the $(i, j)$-entry of $G^{-1}(t)$ so the result follows.                                                                                    □

**Remark 3** With appropriate changes to the setup and following a similar proof, Theorem 5 extends to smooth points on $d$-folds in $\mathbb{R}^n$. We do not consider $d > 2$ here since it remains an open problem to compute a numerical cell decomposition using numerical algebraic geometry for $d > 2$.

**Example 15** To illustrate, consider the ellipsoid $x^2 + 10(y^2 + z^2) = 1$ at

$$p = \begin{bmatrix} 1 \\ 0 \\ 0 \end{bmatrix} \text{ with } w_1 = \begin{bmatrix} 0 \\ 1 \\ 0 \end{bmatrix} \text{ and } w_2 = \begin{bmatrix} 0 \\ 0 \\ 1 \end{bmatrix} \text{ so that } X(t_1, t_2) = \begin{bmatrix} \sqrt{1 - 10(t_1^2 + t_2^2)} \\ t_1 \\ t_2 \end{bmatrix}.$$

**Table 6** Comparison of using the local tangential parameterization on a nine-point stencil with varying values of $a$ when solving (18)

|  | $N$ | $L_\infty$ error | Order |
|---|---|---|---|
| a = 1 | 20 | $3.462 \times 10^{-2}$ | – |
|  | 40 | $8.655 \times 10^{-4}$ | 2.000 |
|  | 80 | $2.164 \times 10^{-4}$ | 2.000 |
|  | 160 | $5.410 \times 10^{-5}$ | 2.000 |
| a = 10 | 20 | $2.337 \times 10^{-2}$ | – |
|  | 40 | $5.756 \times 10^{-3}$ | 2.022 |
|  | 80 | $1.435 \times 10^{-3}$ | 2.004 |
|  | 160 | $4.056 \times 10^{-4}$ | 1.823 |
| a = 50 | 20 | $3.219 \times 10^{-2}$ | – |
|  | 40 | $1.326 \times 10^{-2}$ | 1.279 |
|  | 80 | $3.606 \times 10^{-3}$ | 1.879 |
|  | 160 | $9.129 \times 10^{-4}$ | 1.982 |

Clearly, $X(0,0) = p$. Since $\frac{\partial X_1(t_1,t_2)}{\partial t_i} = \frac{-10t_i}{X_1(t_1,t_2)}$, it is clear that $\frac{\partial X(0,0)}{\partial t_i} = w_i$. Moreover, for $(t_1, t_2)$ near the origin, (4) becomes

$$\Delta u(t_1, t_2) = \sqrt{\frac{1-10(t_1^2+t_2^2)}{1+90(t_1^2+t_2^2)}} \cdot \left[ \frac{\partial}{\partial t_1} \left( \sqrt{\frac{1+90(t_1^2+t_2^2)}{1-10(t_1^2+t_2^2)}} \left( \frac{1-10t_1^2+90t_2^2}{1+90(t_1^2+t_2^2)} \frac{\partial u}{\partial t_1} - \frac{100t_1 t_2}{1+90(t_1^2+t_2^2)} \frac{\partial u}{\partial t_2} \right) \right) \right.$$
$$\left. + \frac{\partial}{\partial t_2} \left( \sqrt{\frac{1+90(t_1^2+t_2^2)}{1-10(t_1^2+t_2^2)}} \left( \frac{1+90t_1^2-10t_2^2}{1+90(t_1^2+t_2^2)} \frac{\partial u}{\partial t_2} - \frac{100t_1 t_2}{1+90(t_1^2+t_2^2)} \frac{\partial u}{\partial t_1} \right) \right) \right]$$

which yields $\Delta u(0,0) = \frac{\partial^2 u(0,0)}{\partial t_1^2} + \frac{\partial^2 u(0,0)}{\partial t_2^2}$ in accordance with Theorem 5.

From an unstructured mesh of points on the surface, one can easily construct a local discretization of $\Delta u$ at each grid point with respect to the local tangential parameterization yielding a linear system to solve as in the curve case.

**Example 16** Consider the following problem

$$-\Delta u + u = f(x, y, z; a) \quad \text{on } x^2 + a(y^2 + z^2) = 1 \tag{22}$$

where $a \in \mathbb{R}_{>0}$ and $f(x, y, z; a) = \frac{1}{3(a+x^2(1-a))^2} \left[ ax(2a+1) + x^3(1-a)(3a+x^2(1-a)) \right]$. The surface is an ellipsoid (shown in Fig. 12) and the choice of $f$ was selected so that (22) has an exact solution of $u(x, y, z) = x/3$ which is used for error analysis. In particular, using a roughly uniform grid of size $N^2$ on the ellipsoid with the local tangential parameterization, the results are summarized in Table 6 using a nine-point stencil for various choice of $a$. Figure 12 shows the solution of (22) computed when $N = 40$.

### 4.3 Local Parameterization Near Singularities

For almost smooth surfaces, there are only finitely many singular points and thus each are isolated. As with the curve case, one first computes a local irreducible component at each singular point since the value of $u$ at a singular point could be different along different local irreducible components. If a local irreducible component has local degree 1, it is locally
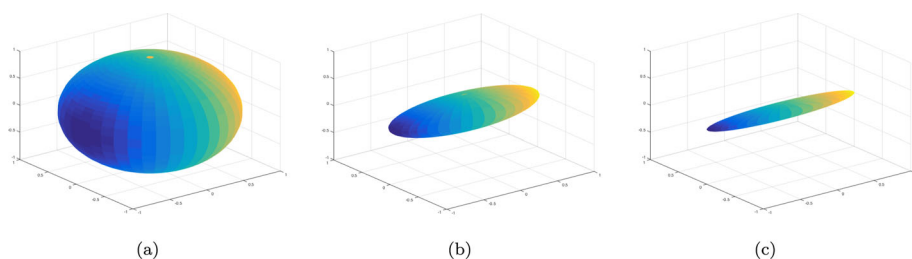
(a)     (b)     (c)

**Fig. 12** Solution of (22) with $N = 40$ for **a** a = 1, **b** a = 10, and **c** a = 50

**Table 7** Error analysis for solving (23)

| $N$ | $L_\infty$ error |
|---|---|
| 20 | $2.235 \cdot 10^{-2}$ |
| 40 | $1.464 \cdot 10^{-3}$ |
| 80 | $3.075 \cdot 10^{-4}$ |
| 160 | – |

diffeomorphic to a well-defined tangent plane for which a local tangential parameterization from Sect. 4.2 can be used. For local irreducible components of higher local degree, one can use a local parameterization (or an approximation of one) to discretize near the singularity for each each local irreducible component.

**Example 17** Consider the following problem

$$- \Delta u + u = x \quad \text{on } (x^2 + y^2 + z^2)^2 - 4(x^2 + y^2) = 0 \qquad (23)$$

where the surface is a called a horn torus (shown in Fig. 13). The horn torus is almost smooth with a singularity at the origin. Using an approximately uniform grid of $N^2$ points, the local tangential parameterization was used away from the origin. The surface is locally irreducible at the origin and the following local parameterization was utilized:

$$x(t_1, t_2) = t_1^2 \cos(t_2), \quad y(t_1, t_2) = t_1^2 \sin(t_2), \quad z(t_1, t_2) = t_1 \sqrt{2 - t_1^2}.$$

A nine-point stencil was used at all points with the results summarized in Table 7 where the error is computed by comparing with the solution computed when $N = 160$. Figure 13 shows the solution of (23) when $N = 40$.

## 5 Conclusion

Traditional approaches for solving elliptic PDEs on manifolds may have difficulty when the domain has singularities since the solution can be multivalued at a singularity. After establishing a theoretical result about well-posedness for curves in Theorem 1, computational approaches for solving elliptic PDEs on real closed algebraic curves and almost smooth surfaces were considered. When a global parameterization is not readily available, a local approach that combines numerical algebraic geometry, differential geometry, and finite differences was described and analyzed. Several examples were used to demonstrate the convergence properties of the numerical scheme. Although the approach could be naturally
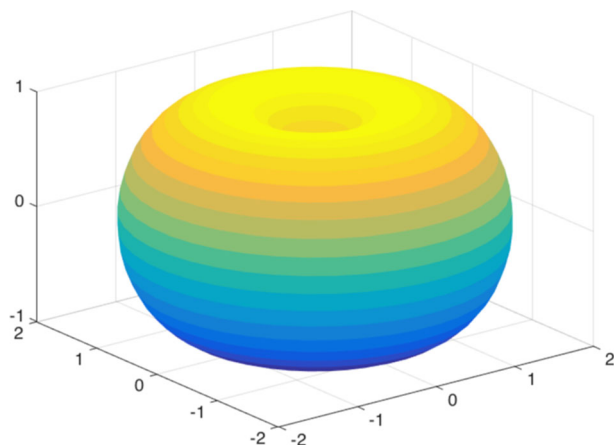
**Fig. 13** Solution for $-\Delta u + u = x$ on $(x^2 + y^2 + z^2)^2 - 4(x^2 + y^2) = 0$ when $N = 40$

extended to domains that are almost smooth real closed algebraic sets of dimension larger than 2, the current challenge for such domains is with computing a cellular decomposition. Additionally, further analysis of elliptic PDEs defined on a surface containing a curve of singularities is warranted.

**Data Availability** Enquiries about data availability should be directed to the authors.

## Declarations

**Conflict of interest** The authors declare that they have no Conflict of interest.

## References

1. Amethyst, S., Hauenstein, J.D., Wampler, C.W.: Cellular decompositions and Chebyshev interpolants for real algebraic curves. Preprint available at www.nd.edu/~jhauenst/preprints/ahwCellDecomp.pdf
2. Bates, D.J., Hauenstein, J.D., Sommese, A.J., Wampler, C.W.: Bertini: software for numerical algebraic geometry. Available at https://bertini.nd.edu/
3. Bates, D.J., Hauenstein, J.D., Sommese, A.J., Wampler, C.W.: Numerically Solving Polynomial Systems with Bertini. SIAM, Philadelphia (2013)
4. Beirao da Veiga, L., Buffa, A., Sangalli, G., Vázquez, R.: Mathematical analysis of variational isogeometric methods. Acta Numer. **23**, 157–287 (2014)
5. Bertalmio, M., Cheng, L.-T., Osher, S., Sapiro, G.: Variational problems and partial differential equations on implicit surfaces. J. Comput. Phys. **174**, 759–780 (2002)
6. Bertalmio, M., Sapiro, G., Cheng, L.-T., Osher, S.: A framework for solving surface partial differential equations for computer graphics applications. UCLA CAM report (00–43) (2000)
7. Besana, G.M., Di Rocco, S., Hauenstein, J.D., Sommese, A.J., Wampler, C.W.: Cell decomposition of almost smooth real algebraic surfaces. Numer. Algorithms **63**(4), 645–678 (2013)
8. Brake, D.A., Bates, D.J., Hao, W., Hauenstein, J.D., Sommese, A.J., Wampler, C.W.: Algorithm 976: Bertini_real: numerical decomposition of real algebraic curves and surfaces. ACM Trans. Math. Softw. **44**(1), 10 (2017)
9. Brake, D.A., Hauenstein, J.D., Sommese, A.J.: Numerical local irreducible decomposition. LNCS **9582**, 124–129 (2016)

10. Burman, E., Hansbo, P., Larson, M.G., Massing, A.: Cut finite element methods for partial differential equations on embedded manifolds of arbitrary codimensions. ESAIM: M2AN **52**, 2247–2282 (2018)
11. Dziuk, G., Elliott, C.M.: Finite element methods for surface PDEs. Acta Numer. **22**, 289–396 (2013)
12. Lai, R., Chan, T.F.: A framework for intrinsic image processing on surfaces. Comput. Vis. Image Underst. **115**, 1647–1661 (2011)
13. Varah, J.M.: A lower bound for the smallest singular value of a matrix. Linear Algebra Appl. **11**(1), 3–5 (1975)
14. Ahlberg, J.H., Nilson, E.N.: Convergence properties of the spline fit. J. Soc. Ind. Appl. Math. **11**(1), 95–104 (1963)
15. Lu, Y., Bates, D.J., Sommese, A.J., Wampler, C.W.: Finding all real points of a complex curve. In: Algebra, Geometry and Their Interactions, vol. 448 of Contemporary Mathematics. AMS, Providence, pp. 183–205 (2007)
16. Meyer, M., Desbrun, M., Schroder, P., Barr, A. H.: Discrete differential-geometry operators for triangulated 2-manifolds. In: Hege, H.C., Polthier, K. (eds.) Visualization and Mathematics III. Springer, New York, pp. 35–57 (2003)
17. Osher, S., Sethian, J.: Fronts propagation with curvature-dependent speed: algorithms based on Hamilton–Jacobi formulations. J. Comput. Phys. **79**, 12–49 (1988)
18. Reuter, M., Wolter, F., Peinecke, N.: Laplace–Beltrami spectra as shape-DNA of surfaces and solids. Comput. Aided Des. **38**, 342–366 (2006)
19. Sommese, A.J., Wampler, C.W.: The Numerical Solution of Systems of Polynomials Arising in Engineering and Science. World Scientific Publishing Co. Pte. Ltd., Hackensack (2005)
20. Spira, A., Kimmel, R.: Geometric curve flows on parametric manifolds. J. Comput. Phys. **223**, 235–249 (2007)
21. Taubin, G.: Geometric signal processing on polygonal meshes. In: Eurographics State of the Art Reports, vol. 4, pp. 81–96 (2000)
22. Wang, Y., Lui, L.M., Gu, X., Hayashi, K.M., Chan, T.F., Toga, A.W., Thompson, P.M., Yau, S.: Brain surface conformal parameterization using Riemann surface structure. IEEE Trans. Med. Imaging **26**, 853–865 (2007)
23. Xu, G.: Convergent discrete Laplace–Beltrami operators over triangular surfaces. In: Proceedings of Geometric Modeling and Processing. IEEE, pp. 195–204 (2004)